Superresolution Imaging of Optical Vortices in a Speckle Pattern

Marco Pascucci,[1] Gilles Tessier,[2] Valentina Emiliani,[1] and Marc Guillon[1,*]
[1]Wavefront Engineering Microscopy Group, Neurophotonics Laboratory, CNRS UMR 8250, Paris Descartes University, Sorbonne Paris Cité, Paris 75006, France
[2]Holographic Microscopy Group, Neurophotonics Laboratory, CNRS UMR 8250, Paris Descartes University, Sorbonne Paris Cité, Paris 75006, France
(Received 17 September 2015; published 4 March 2016)

We characterize, experimentally, the intensity minima of a polarized high numerical aperture optical speckle pattern and the topological charges of the associated optical vortices. The negative of a speckle pattern is imprinted in a uniform fluorescent sample by photobleaching. The remaining fluorescence is imaged with superresolution stimulated emission depletion microscopy, which reveals subdiffraction fluorescence confinement at the center of optical vortices. The intensity statistics of saturated negative speckle patterns are predicted and measured. The charge of optical vortices is determined by controlling the handedness of circular polarization, and the creation or annihilation of a vortex pair along propagation is shown.

DOI: 10.1103/PhysRevLett.116.093904

Propagation of coherent waves in random scattering media is associated with the generation of speckle patterns. For scalar wave fields; these speckle patterns contain hot spots but, also, true zeros of the field where the phase is singular [1]. These phase singularities—or phase dislocations—exhibit spiral structures with topological charges $+1$ and -1 [2]. The associated zeros of intensity surrounded by light are called optical vortices because of the circular optical current circulating around their dark center [3]. The vortex centers draw lines in space which may loop and knot [2,4] and which can be seen as the wire frame or the "skeleton" onto which the field is built [5]. The information about the circulation handedness of the optical current around these lines lies in the phase of the field.

In any speckle pattern, the density of nodal points is the same as the density of hot spots [6,7]. However, the separation distance between phase singularities can be arbitrarily small, especially when two vortices of opposite charges approach and annihilate, or nucleate and split apart [8]. In addition, the three vector components of an optical field may hang on different nodal skeletons, making the characterization of zeros complicated. For these two reasons, former experimental characterizations of phase singularities in vectorial electromagnetic waves were performed with polarized beams of low numerical aperture (NA) [7,9], or considering a single vector component of the field [10–12] in order to remain within the validity of the scalar approximation.

However, the most promising applications of complex vector fields involve high NA beams and lie beyond the scalar approximation. For instance, phase dislocations are typically used in superresolution microscopy in order to create saturating intensity patterns with perfect zeros [13–16]. Specifically, in stimulated emission depletion (STED) microscopy [13,17], an optical vortex is commonly used, in combination with a circular polarization, to cancel the axial component of the field at the vortex center [18,19]. In high NA optical speckle fields, the joint characterization of optical vortices and intensity minima remains unexplored, notably due to the subdiffraction spatial scales involved.

In this Letter, we report on the characterization of intensity minima and optical vortices in polarized high NA random speckle patterns using superresolution STED microscopy. To do so, the negative of the speckle pattern is first recorded by photobleaching a uniformly fluorescent sample. Saturated bleaching leaves fluorescent spots at intensity minima, whose size and spacing may decrease below the diffraction limit, thus, requiring superresolution microscopy. First, we experimentally validate an analytical model which quantifies the intensity statistics of the negative. Then, after characterizing the subdiffraction confinement of fluorescence at a vortex of a speckle pattern, we demonstrate that the topological charge of the optical vortices associated with intensity minima can be revealed, experimentally, by controlling the polarization of the random beam. This identification allows visualizing the creation or annihilation of a vortex pair of opposite charges. Finally, we quantify, analytically, the amplitude of the axial component of a circularly polarized random wave field with Gaussian statistics.

The negative of a speckle pattern was first recorded by photobleaching a uniformly fluorescent layer of poly-D-lysine (Sigma-Aldrich) deposited on a coverslip and covalently labeled with the organic dye ATTO 532 (ATTO-TEC) functionalized with an N-Hydroxysuccinimide (NHS) ester group. Photobleaching was performed at 403 nm using a spatial light modulator (SLM) to generate speckle patterns

of controlled statistics and size. The SLM was conjugated to the back focal plane of the microscope objective using a telescope to obtain a bleaching beam with $NA_s = 0.45$. The bleaching beam was circularly polarized before entering the objective lens. The phase pattern displayed on the SLM was generated in order to obtain fully developed speckles with Gaussian statistics over a 5 μm-wide surface in the sample. The bleaching light power was 2.0 mW in the sample plane and bleaching time provided a control over the total radiation fluence. After photobleaching the sample, super-resolution imaging was performed on the same system with a custom built STED microscope [17] by combining beam paths with dichroic beam splitters [20]. Imaging was performed through the same 1.4 NA microscope objective as used for photobleaching. The excitation beam was obtained by filtering a supercontinuum laser source through a 480/20 filter and combined with the 15 mW depleting beam at 620 nm by dichroic beam splitters.

To characterize the negatives of speckle patterns, first, we study the probability density function (PDF) of the remaining fluorescence intensity after photobleaching. Experimentally, these PDFs are measured in STED images. An illustration of STED fluorescence images obtained after photobleaching is shown in Figs. 1(a) and 1(b) for average

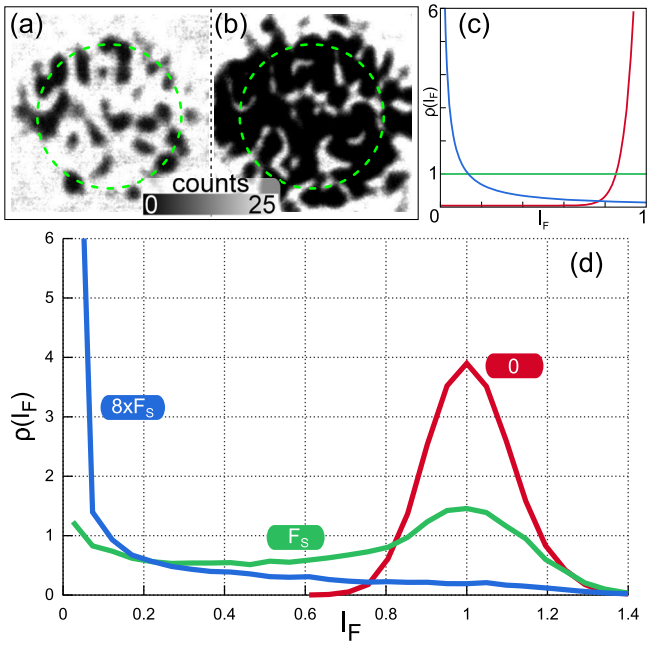

FIG. 1. Remaining fluorescence after photobleaching the fluorescent sample with 5 μm spots having fluences (a) $F_s = 1.6\ \mathrm{mJ}\cdot\mu\mathrm{m}^{-2}$ and (b) $8F_s = 12.8\ \mathrm{mJ}\cdot\mu\mathrm{m}^{-2}$. Scale bar is 1 μm. (c) Intensity PDFs expected from a uniform sample and a one-photon bleaching model for average saturation parameters $r = 0.01$ (red), $r = 1$ (green), and $r = 8$ (blue). (d) The experimental intensity PDFs of negative speckle patterns are plotted for the region marked by the dashed circle in (a) and (b) [for fluences $\langle F\rangle = 0$ (red), $\langle F\rangle = F_s$ (green), and $\langle F\rangle = 8F_s$ (blue)].

radiation fluences $1.6\ \mathrm{mJ}\cdot\mu\mathrm{m}^{-2}$ and $12.8\ \mathrm{mJ}\cdot\mu\mathrm{m}^{-2}$, respectively. In these experiments, photobleaching involves the transition from the fluorescent excited state towards a long-living dark state. The PDF of fluorescence intensity is discussed in the light of a one-photon bleaching model with constant quantum yield. For a fully developed speckle pattern, the PDF of the excitation intensity I_e is $\rho(I_e) = (1/\langle I\rangle)\exp[(-I_e/\langle I\rangle)]$ where $\langle I\rangle$ is the average speckle intensity. In our case, $\langle I\rangle$ ($\approx 10\ \mathrm{kW}\cdot\mathrm{cm}^{-2}$) is more than 3 orders of magnitude smaller than the absorption saturation intensity of the dye I_s, yielding a population in the excited level proportional to the illumination intensity. Therefore, the population remaining in the fluorescent state N_f decreases exponentially with the radiation fluence $F = I_e \times t$: $N_f \propto \exp(-qF/I_s)$, where q is the transition rate from the excited level to the dark state. The negative of a speckle pattern is also a fluorescent speckle pattern of intensity I_f ($\propto N_f$). In the frame of this model, the PDF of I_f in the sample can be analytically written as

$$\rho(I_f) = \frac{{I_f}^{(1/r)-1}}{r},$$

where r is the average saturation parameter: $r = qt\langle I\rangle/I_s = \langle F\rangle/F_s$, with $F_s = I_s/q$ the saturation fluence of the transition and $\langle F\rangle = \langle I\rangle \times t$ the average fluence. Here, the fluorescence intensity in the absence of bleaching is normalized.

An illustration of this distribution is given in Fig. 1(c) for $r \in \{0.01, 1, 8\}$. Interestingly, for $r = 1$, we get $\rho(I_f) = \mathbb{1}$, the PDF of the luminescent fluorophore concentration in the sample is then expected to be uniform. Experimentally, this plateau is observed for an average radiation fluence $1.6\ \mathrm{mJ}\cdot\mu\mathrm{m}^{-2}$ [as shown in Fig. 1(d)] which may then be identified to the saturation fluence F_s.

Photobleaching is associated with a decrease of the typical size of the remaining fluorescent structures with bleaching time [Figs. 1(a) and 1(b)]. In particular, at optical vortices of the transverse components of the bleaching field, bright fluorescent spots remain and may decrease in size to arbitrarily low dimensions. As shown in the context of reversible saturable optical fluorescence transitions (RESOLFT) superresolution imaging, subdiffraction fluorescence confinement scales as [15]

$$d = \frac{d_0}{\sqrt{1 + r_s}}, \tag{1}$$

where d_0 is the size of the excitation spot and r_s is the saturation factor of the optical transition to the dark state. In our case, $r_s = F/F_s$ where F is the local radiation fluence. Since d can be much smaller than d_0, the characterization of subdiffraction fluorescence confinement by optical vortices of the speckle pattern requires superresolution microscopy. Our STED microscope reaches resolutions down to 45 nm

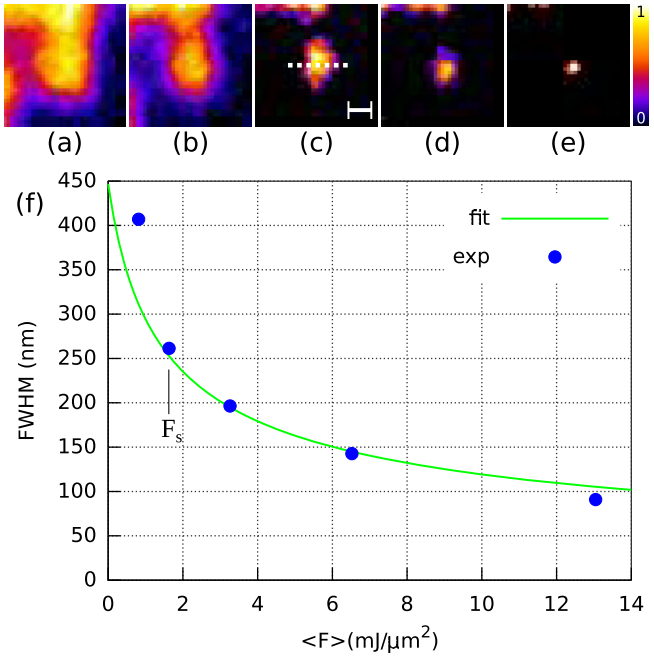

FIG. 2. Sequence of a uniformly fluorescent layer gradually photobleached with a speckle pattern (a)–(e) and evolution of the FWHM of the remaining fluorescent spot as a function of bleaching time (f). The FWHM is plotted along the dashed line in (c). The scale bar corresponds to 200 nm. Each image is normalized and uses the same color bar. The peak intensity of the remaining spot in (e) is approximately 30% of the peak intensity in (a). Bleaching is performed with average radiation fluences $\langle F\rangle \in \{F_s/2, F_s, 2F_s, 4F_s, 8F_s\}$. The continuous line is a fit using Eq. (1) with fitting parameter $F/\langle F\rangle = 2.1$.

[17], below the typical size of the remaining fluorescent structures we analyze. An illustration of a sequence of the saturated negative speckle pattern is shown in Figs. 2(a)–2(e) for average radiation fluences $\langle F\rangle$ varying from $F_s/2$ to $8F_s$ with a geometric progression, demonstrating fluorescence confinement. The evolution of the full width at half maximum (FWHM) d of the remaining fluorescent spot shown in Figs. 2(a)–2(e), is then plotted [Fig. 2(f)] as a function of the average radiation fluence $\langle F\rangle$ in the speckle pattern. Since the local fluence F is unknown, its value is fitted using Eq. (1), setting $d_0 = \lambda/(2\mathrm{NA_s}) = 450$ nm. For an average radiation fluence $\langle F\rangle = 8F_s$, a spot size of 80 nm FWHM is obtained, more than a factor of 5 below d_0.

When selectively saturating an optical transition with a beam of high NA, the axial field cannot be neglected. In STED microscopy, for example, the depleting toroidal beam is usually an optical vortex of charge 1 generated by a helicoidal phase mask [15]. While a circular polarization of the proper handedness cancels the axial field [18,19], choosing the opposite handedness results in a nonzero axial component at the focus, which suppresses fluorescence at the torus center. Speckle patterns naturally contain vortex phase singularities of charge $+1$ and -1 [2].

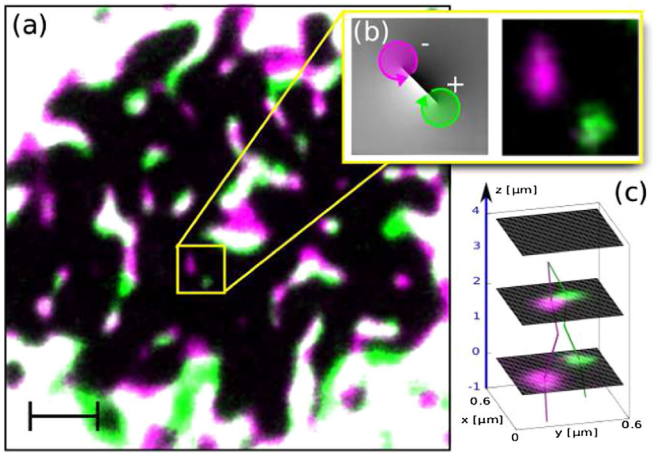

FIG. 3. Overlay of the STED images of two regions bleached with a single scattering phase pattern but with two orthogonal circular polarizations (a) (radiation fluence is $8F_s = 12.8\,\mathrm{mJ}\cdot\mu\mathrm{m}^{-2}$). Circular polarization allows identifying the charge of phase vortices. Two phase vortices of opposite charge are identified (b). Axial displacement of the bleaching pattern by steps of 1 μm reveals the annihilation of this pair of optical vortices with propagation (c). The handedness of phase vortices is identified by the handedness of circular polarization. Scale bars: (a) 1 μm, (b) 200 nm.

Therefore, a speckle pattern generated by a beam passing through a random phase mask and focused with a right-handed circular polarization will have a minimized axial field at right-handed optical vortices and a maximized axial field at its left-handed ones. We demonstrate this phenomenon experimentally in Fig. 3(a) where the overlay of the two STED images reveals that, for the two polarizations, dark spots of the speckle appear at different locations. This result demonstrates that the handedness of polarization plays an essential role on speckle intensity, mainly on the contribution of the axial field. The remaining fluorescent points may, thus, be interpreted as the locations of right- and left-handed vortex phase singularities of the transverse field. In Fig. 3(b), two phase vortices of opposite charges are shown and illustrated with a simulated compatible phase pattern.

Moreover, vortex phase dislocations may annihilate and create in pairs by conserving the total charge [8]. Tracking these phase dislocations along the propagation axis is also possible by recording them at several axial positions with respect to the bleaching beam. STED imaging is then performed placing the sample back in the focal plane. Along the propagation axis, two optical vortices of opposite charges are observed to annihilate: their trajectories are shown in Fig. 3(c) where the two vortices were imaged in six planes with a micron step from $z = -1$ to $z = +4$ μm. Before annihilation, we measured that the separation distance between the two vortices at $z = +2$ μm is as close as 140 nm, more than a factor of 3 below d_0 and, thus, well below the diffraction limit.

The former experimental results demonstrate the possibility to selectively minimize or maximize the axial field at optical vortices of the speckle pattern. Therefore, we now aim at characterizing, quantitatively, the magnitude of the axial component of the field at zeros of its transverse components depending on the charge of the singularity. In principle, circular polarization may ensure perfect cancellation of the axial field at the center of an optical vortex if the phase increases uniformly along the azimuthal coordinate. However, optical vortices appearing in fully developed speckles exhibit an elliptical phase modulation along the azimuthal coordinate [2]. In the case of a fully developed speckle pattern exhibiting Gaussian statistics, the axial field at optical vortices can be calculated analytically [21]. For a right-handed circular polarization of the beam, the calculation yields the PDFs $\rho_L(I_z)$ and $\rho_R(I_z)$ of I_z at the center of left-handed and right-handed optical vortices of the transverse field, respectively,

$$\rho_R(I_z) = \frac{k^2}{2b}\exp\left(-\frac{k^2 I_z}{2b}\right), \tag{2}$$

$$\rho_L(I_z) = \frac{k^2}{2b}\exp\left(-\frac{k^2 I_z}{4b}\right)\left[1-\exp\left(-\frac{k^2 I_z}{4b}\right)\right], \tag{3}$$

where b depends on the power spectrum of the speckle field and is proportional to the average intensity $\langle I\rangle$ [21].

Curves corresponding to Eqs (2) and (3) are shown in Fig. 4 for a 0.45 NA optical field with right-handed polarization in an $n = 1.51$ immersion medium (in agreement with the experimental configuration where $\mathrm{NA}_s = 0.45$). The average values of I_z at $+1$ and -1 vortices are, then, $\langle I_z^-\rangle = 3\langle I_z^+\rangle = \frac{3}{4}(\mathrm{NA}_s/n)^2\langle I\rangle$, in a 1 to 3 ratio. However, comparing average values is not relevant when discussing a saturated process: the relevant values to compare here are $\rho_L(0)$ and $\rho_R(0)$. For subdiffraction fluorescence confinement with saturation parameter r, fluorescence will be preserved if I_z is typically smaller than $\langle I\rangle/r$. Therefore, bright spots associated with right-handed optical vortices dominate under saturated conditions.

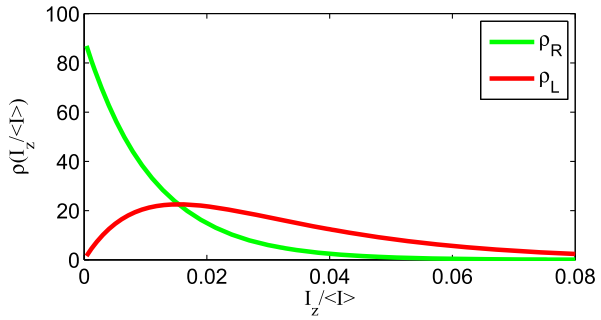

FIG. 4. Probability density functions ρ_L and ρ_R of the intensity of the axial component of the field at left- and right-handed vortex phase singularity locations of the transverse components for a right-handed circularly polarized random wave with Gaussian statistics. The refractive index of the medium is $n = 1.51$ and numerical aperture $\mathrm{NA}_s = 0.45$ in agreement with experimental conditions.

Interestingly, increasing the NA of the speckle pattern increases the spatial density of phase singularities as $(\mathrm{NA}_s/n)^2$, like the magnitude of the intensity at phase vortices, according to the former calculations. Consequently, for a given average fluence $\langle F\rangle$, the spatial density of remaining fluorescent spots after saturated photobleaching is expected to be invariant under changes of (NA_s/n).

In conclusion, we characterized the statistics of negatives of fully developed speckle patterns. We demonstrated subdiffraction confinement of fluorescence at the minima of a 0.45 NA speckle beam, validating the same law as established for RESOLFT microscopy [15]. We showed that it is possible to selectively maintain fluorescence ability at positively—or negatively—charged vortex phase singularities of the transverse components of the field by controlling the handedness of circular polarization. Thus, it was possible to identify the charge of optical vortices. An annihilation between two vortices of opposite charges was shown along propagation. Finally, we estimated, analytically, the amplitude of intensity minima of a polarized speckle pattern. We point out that arguments developed in this Letter rely on a first order approximation in (NA/n), which predicts a change of the axial field with the handedness of circular polarization proportional to (NA/n). Conversely, the power expansion of the transverse components does not contain a first order term and can be considered as a polarization invariant at the first order.

Finally, subdiffraction confinement of fluorescence demonstrates the ability of high numerical speckle fields to behave like multidonut structures like those used in parallelized RESOLFT microscopes [16,23]. In analogy with speckle imaging modalities allowing imaging behind opaque media [24], the saturation of an optical transition with speckle structures should, thus, allow parallelized superresolution speckle imaging. In this case, a reversible transition would be required as in other RESOLFT microscopy techniques. Namely, speckle illumination could be used to saturate fluorescence excitation [14], stimulated emission [13], or any reversible photoswitching mechanism [25].

The authors thank Cécile Jouffret for preparing the polylysine samples, and Marcel Lauterbach for helping with the experimental setup and for comments on the manuscript. They also thank Benoît C. Forget and Rémi Carminati for stimulating discussions. This work was supported by grants from the Région Ile-de-France. We acknowledge funding by the Paris School of Neuroscience (ENP), the Agence Nationale de la Recherche (Grant No. ANR-10-INSB-04-01) and France-BioImaging infrastracture network.

*Corresponding author.
marc.guillon@parisdescartes.fr

[1] J. Nye and M. Berry, Proc. R. Soc. A **336**, 165 (1974).
[2] M. Berry and M. Dennis, Proc. R. Soc. A **456**, 2059 (2000).
[3] M. V. Berry, J. Opt. A **11** (2009).
[4] K. O'Holleran, M. R. Dennis, and M. J. Padgett, Phys. Rev. Lett. **102**, 143902 (2009).
[5] M. Berry and M. Dennis, Proc. R. Soc. A **457**, 2251 (2001).
[6] M. V. Berry, J. Phys. A **11**, 27 (1978).
[7] N. Baranova, B. Zel'dovich, A. Mamaev, N. Pilipetskii, and V. Shkukov, JETP Lett. **33**, 195 (1981).
[8] J. Nye, J. Hajnal, and J. Hannay, Proc. R. Soc. A **417**, 7 (1988).
[9] J. Leach, M. R. Dennis, J. Courtial, and M. J. Padgett, New J. Phys. **7**, 55 (2005).
[10] J. Nye, M. Berry, and M. Walford, Nat. Phys. **240**, 7 (1972).
[11] S. Zhang and A. Z. Genack, Phys. Rev. Lett. **99**, 203901 (2007).
[12] S. Zhang, B. Hu, P. Sebbah, and A. Z. Genack, Phys. Rev. Lett. **99**, 063902 (2007).
[13] S. Hell and J. Wichmann, Opt. Lett. **19**, 780 (1994).
[14] M. Gustafsson, Proc. Natl. Acad. Sci. U.S.A. **102**, 13081 (2005).
[15] B. Harke, J. Keller, C. K. Ullal, V. Westphal, A. Schoenle, and S. W. Hell, Opt. Express **16**, 4154 (2008).
[16] A. Chmyrov, J. Keller, T. Grotjohann, M. Ratz, E. d'Este, S. Jakobs, C. Eggeling, and S. W. Hell, Nat. Methods **10**, 737 (2013).
[17] M. A. Lauterbach, M. Guillon, A. Soltani, and V. Emiliani, Sci. Rep. **3**, 2050 (2013).
[18] X. Hao, C. Kuang, T. Wang, and X. Liu, J. Opt. **12**, 115707 (2010).
[19] S. Galiani, B. Harke, G. Vicidomini, G. Lignani, F. Benfenati, A. Diaspro, and P. Bianchini, Opt. Express **20**, 7362 (2012).
[20] M. A. Lauterbach, M. Guillon, and V. Emiliani (to be published).
[21] See Supplemental Material at http://link.aps.org/supplemental/10.1103/PhysRevLett.116.093904, for the description of the main steps of the calculation, which includes Ref. [22].
[22] J. W. Goodman, *Speckle Phenomena in Optics* (Roberts and Co., Englewood, CO, 2006), Chap. 4, p. 122.
[23] B. Yang, F. Przybilla, M. Mestre, J.-B. Trebbia, and B. Lounis, Opt. Express **22**, 5581 (2014).
[24] J. Bertolotti, E. G. van Putten, C. Blum, A. Lagendijk, W. L. Vos, and A. P. Mosk, Nature (London) **491**, 232 (2012).
[25] S. W. Hell, Phys. Lett. A **326**, 140 (2004).